ISSN: 2639-0108

Research Article

Advances in Theoretical & Computational Physics

Quantum Zeno Jumps in a Resonantly Driven Qubit under Frequent Measurements

Gilbert Reinisch[1,2]

[1]*Université de la Côte d'Azur - Observatoire de la Côte d'Azur 06304 Nice Cedex – France*

[2]*Science Institute, University of Iceland, Dunhaga 3, IS-107 Reykjavik, Iceland*

***Corresponding author**

Gilbert Reinisch, Université de la Côte d'Azur - Observatoire de la Côte d'Azur 06304 Nice Cedex – France and Science Institute, University of Iceland, Dunhaga 3, IS-107 Reykjavik, Iceland.

Submitted: 12 July 2021; **Accepted:** 19 July 2021; **Published:** 26 July 2021

Citation: *Gilbert Reinisch. (2021). Quantum Zeno Jumps in a Resonantly Driven Qubit under Frequent Measurements. Adv Theo Comp Phy, 4(3), 234-240.*

Abstract

In Nature, 570, 200 (2019), Minev and co-authors' experiment shows how to deterministically "catch and reverse a quantum jump mid-flight" in a continuously-observed Rabi-stimulated qubit. Its interpretation is in debate (La Recherche, 555, 40, (2020)). We show that the quantum Zeno effect (QZE) of continuous measurement —by use of photon emission from a 3rd high-rate monitored ancilla level— can be described by an action-angle canonical transformation of the original Hamiltonian dynamical system (HDS) theory of QZE. Then energy whose mean value yields the well-known resonant Rabi harmonic dynamics is actually defined by large-amplitude high-frequency oscillations of the internal as well as of the overall phase of the two-level system. By making use of their standard deviation, we show that the separatrix crossing of the HDS trajectory yields the quantized action nh where n = 1, 2, 3 .... Therefore, the jump dynamics observed in Minev et al. experiment belongs to a series of discrete quantum jumps: it corresponds in this experiment to n = 3.

PACS numbers: 02.60.Lj 12.20.Ds 73.21.La

Introduction

According to the quantum Zeno effect (QZE), frequent (almost continuous) measurements would inhibit the decay of unstable quantum systems [1]. It is usually explained by two properties [2, 3]: (i) the Schrödinger equation which ensures that the speed of transition to the other states at t = 0 is zero (hence the decay probability is $\alpha\ t^2$); (ii) the system evolves from the same initial state after every measurement. This latter condition yields the controversial interpretation of QZE [4, 5]. Indeed, according to some authors [6, 7], the QZE is a pure dynamical process which does not involve any projection operator while according to the quantum measurement theory [8], the wave-function collapse takes place as a consequence of observation and, consequently, the density matrix of the system loses its off-diagonal components. This latter interpretation has been experimentally verified by use of a Rabi driven two-level system —namely, a ground state |G> and an excited state |D>— with the addition of a 3rd "ancilla" state |B> that actually plays the role of the continuously-operating ground-state population measurement [3, 9, 10]. Specifically, state |B> is connected by a strongly allowed transition to level |G> and it can decay only to |G>. The continuous state measurement is carried out by resonantly (Rabi) driving the G → B transition with an appropriately designed optical pulse. This measurement causes a collapse of the wave function. If the system is projected into the ground-state level |G> at the beginning of the pulse, it cycles between |G> and |B> and emits a series of photons —hence the label |B> for "bright"— until the pulse is turned off. If it is projected into the excited level |D> (for "dark"), it scatters no photons. Therefore, the wave-function collapse is due to a null measurement [11, 12]. That is, the absence of scattered photons when the optical pulse is applied is enough to cause a collapse of the wave function to level |D> [10].

The results of a recent remarkable experiment using a *similar* experimental setup as in QZE pioneering paper [10] with the *same* underlying physical principle have been explained quite successfully by the theory of quantum trajectories [13, 14] *without* any explicit reference to QZE [15]. However, the leader of this experimental group unambiguously states: *"Naturally, our work is directly related to the QZE which applies to both types of jumps"* [16]. Therefore, the purpose of the present paper is to recover by the sole use of QZE the existence of the abrupt jumps between |G> and |D> described in Figures 2a and 3b of experiment [15].

Specifically, this experiment shows the evolution of the state of an unstable two-level system (or qubit), the ground state |G> of which is short-lived since it decays to the third, upper level |B> to which it is connected by a strong resonant field. The condition to observe the evolution found in Figures 2a and 3b of [15] is that the decay rate of |G> be much greater than the Rabi frequency for the qubit (if this condition is violated, the evolution would have a quite different form). This means that the resulting photon emission due

to the G → B transition is quasi-continuous within the time scale of the Rabi period. Thence, it yields indeed the QZE measurement process of the population of unstable ground state |G> displayed in [10]. However, the discovery of the sharp quantum jumps between |G> and |D> in the long-range evolution of the system [15] seems to contradict the very definition of QZE where unstable systems should not decay [1]. Instead of following the well-known standard harmonic decay rate of the Rabi-driven ground state |G> in the absence of any measurement process and its subsequent harmonic probability of finding the system in the excited state |D>, the system should tend to remain "frozen" in |G> when the number of equally spaced measurements increases [10]. Experiment [15] clearly shows that this is not the case. We wish to provide here empirical evidence to support the existence of these anomalous quantum jumps by the use of QZE and first principles; namely: i) a longrange *QZE vs Rabi* competition between stimulated harmonic Rabi transition and QZE population freezing; ii) action quantization in order to select the corresponding Hilbert paths in the appropriate energy spectrum. This approach offers the experimental prediction of the existence of a possible discrete series $n = 1, 2, 3...$ of QZE-vs-Rabi quantum jumps —which we call "quantum Zeno jumps"— of the type shown in Figures 2a and 3b of [15]. In this latter case, we find $n = 3$.

In order to define the action of the system, we use the canonical action-angle Hamiltonian dynamical description of QZE where the Rabi oscillations of the mean energy of the system (which is a very old and well-studied topic in a rotating frame) are taken into account in their non-rotating (original) frame. The interest of this apparently more complicated method is to display by use of the strongly time-dependent internal and overall phases of the two-level system [17] the surprisingly large standard deviation of its energy with respect to the Rabi harmonic mean value: see Figure 7 below. Then this large available energy range defines the discrete quantum Zeno jumps in their appropriate Hilbert space. It is worth noting that, contrary to intuitive opinions, the dynamics of the overall phase of a quantum state can indeed yield an observable physical effect (e.g. it causes the famous 4π-symmetry of spinor wave functions that have been directly verified in both division-of-amplitude [18, 19] and division-of-wave-front [20] neutron interferometry experiments).

We believe that this new scope concerning experiment [15] sheds an interesting light on the art of manipulating qubits where a continuous feedback between basic science and technology is essential. Questions at the foundations of quantum mechanics, which had been put to rest by most physicists in the 1930s, were revisited starting primarily in the 1960s and put to the test in the 1970s, 1980s, and 1990s. Of special interest in the present case: do quantum jumps occur and how does a quantum measurement occur in continuous time [21].

The Hamiltonian dynamical system (HDS)

Following [17], we adopt a two-state Hamiltonian H that is defined by the two Pauli matrices σ_x and σ_z. The corresponding Schrödinger equation for the two-component normalized spinor wave function $\Psi = \{\psi_a, \psi_b\}$ becomes:

$$i\hbar\frac{\mathrm{d}\psi_a}{\mathrm{d}t} = E(t)\psi_a(t) + K\psi_b(t) \quad ; \quad i\hbar\frac{\mathrm{d}\psi_b}{\mathrm{d}t} = -E(t)\psi_b(t) + K\psi_a(t). \tag{1}$$

Note that $\mathbf{H}_{aa} = -\mathbf{H}_{bb} = E(t)$ defines the external drive while $\mathbf{H}_{ab} = \mathbf{H}_{ba} = K$ is real-valued and constant. It defines half the energy gap of the system. We introduce the time-dependent internal and overall phases $\delta(t)$ and $\Theta(t)$ according to:

$$\psi_a(t) = \sqrt{\frac{1+\alpha(t)}{2}}e^{i\Theta(t)} \quad ; \quad \psi_b(t) = \sqrt{\frac{1-\alpha(t)}{2}}e^{i[\Theta(t)+\delta(t)]}. \tag{2}$$

Ansatz (2) in (1) yields the non-autonomous Hamiltonian dynamical system (HDS):

$$\dot{\alpha} = -\frac{\partial\mathcal{H}}{\partial\delta} = \sqrt{1-\alpha^2}\sin\delta \quad ; \quad \dot{\delta} = \frac{\partial\mathcal{H}}{\partial\alpha} = -\frac{\alpha}{\sqrt{1-\alpha^2}}\cos\delta + B, \tag{3}$$

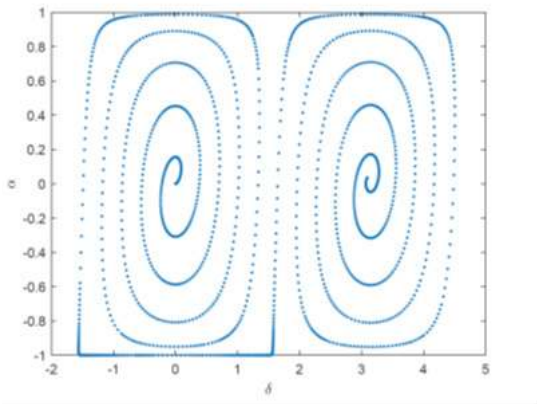

Figure 1: First half Rabi period $2\pi/A$ with $A = 0.1$: desexcitation HDS trajectory starting counter clockwise at $\alpha(0) = \delta(0) = 0$ —i.e. at the fixed point corresponding to the eigenvalue +1— and ending clockwise at $\alpha(2\pi/A) = 0$, $\delta(2\pi/A) = \pi$ —i.e. at the eigenvalue -1, according to (4). The excitation path —namely, the 2nd half of the Rabi period— is the "return" HDS trajectory topologically similar to the above 1rst half one: it starts clockwise at the previous fixed point $\alpha(2\pi/A) = 0$, $\delta(2\pi/A) = \pi$ and ends counter-clockwise at the initial fixed point $\alpha(4\pi/A) = \delta(4\pi/A) = 0$.

defined by the HDS Hamiltonian:

$$\mathcal{H} = \sqrt{1-\alpha^2}\cos\delta + \alpha B, \tag{4}$$

related to the qubit Hamiltonian **H**:

$$K\mathcal{H} = <\Psi|\mathbf{H}|\Psi> . \tag{5}$$

Therefore, the HDS Hamiltonian $\mathcal{H}$ is the quantum expectation value of the qubit energy. The dynamics of the overall phase $\Theta(t)$ is not a 3rd independent variable: it is given by:

$$-\frac{1}{2}\left[\sqrt{\frac{1-\alpha}{1+\alpha}}\cos\delta + B\right]. \tag{6}$$

The reduced drive is defined by $B(t) = E(t)/K$ and the dot means the derivation with respect to the dimensionless time $\tau = \Omega t$ related to the Larmor frequency of the system $\Omega = 2K/\hbar$.

Therefore, we have transformed by use of (2) the two-state spinor quantum system (1) —or qubit— into the mere classical dynamical system (3-4) where for convenience:

$$K = 1 \quad ; \quad \hbar = 2 \quad ; \quad \Omega = 1. \tag{7}$$

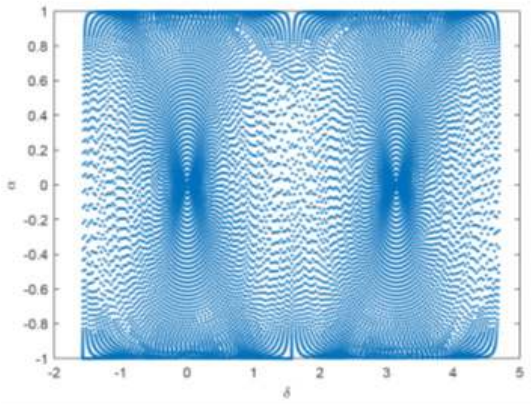

Figure 2: The same as in Figure 1 with A = 0.01. Now the 2nd half Rabi period HDS trajectory will end up at $\alpha(4\pi/A) = 0$, $\delta(4\pi/A) = 2\pi$ instead of $\delta(4\pi/A) = 0$ as in Figure 1.

This HDS may exhibit all types of classical trajectories in its appropriate $\{\alpha \text{ vs } \delta\}$ phase space that is defined by the two canonical variables α and δ (e.g. a resonant Rabi drive yields an aperiodic fractal spectrum [22]) provided the (square) amplitudes (2) yields the respective probabilities for any distribution of observables corresponding to these HDS trajectories.

Assuming as in [15] a weak *resonant* Rabi drive $B(\tau) = A\sin\tau$ with $A << 1$, Figure 1 displays the HDS trajectory for A = 0.1 over one half Rabi period $2\pi/A$, to be compared with Figure 2 when $A = 0.01$. As emphasized in [17], the phase space $\{\alpha$ vs $\delta\}$ is divided into cells of width π and height $2 = \pm 1$, each cell corresponding to 1/4th of a Rabi period. These cells are centered about the fixed points ± 1 which define the eigenvalues in units (7). Following a dense series of quasi-periodic HDS orbits in the $A << 1$ weakly driven case, the trajectory spirals out of one given cell and in into either the next left-hand side or right-hand side one (or reverse). The smaller A, the higher the density of such quasi-periodic orbits whose period approaches closer and closer the A = 0 conservative value ~ 2π: compare Figure 1 and 2. The separatrices between these cells are located at $\alpha = 0$ and $\delta = \pi/2$ (mod. $\pm\pi$) and yield in agreement with definitions (2) an extremely fast flipping of the system between its two states with the period ~ 2π << Rabi period $4\pi/A$: see Figure 3.

The energy of the Rabi-driven two-level system

The time-dependent qubit energy (5) is [17]:

$$K\mathcal{H} = <\Psi|\mathbf{H}|\Psi> = |\psi_a|^2 E_a + |\psi_b|^2 E_b, \tag{8}$$

Where

$$E_a = K\frac{\mathcal{H}+B}{1+\alpha} \quad ; \quad E_b = K\frac{\mathcal{H}-B}{1-\alpha}. \tag{9}$$

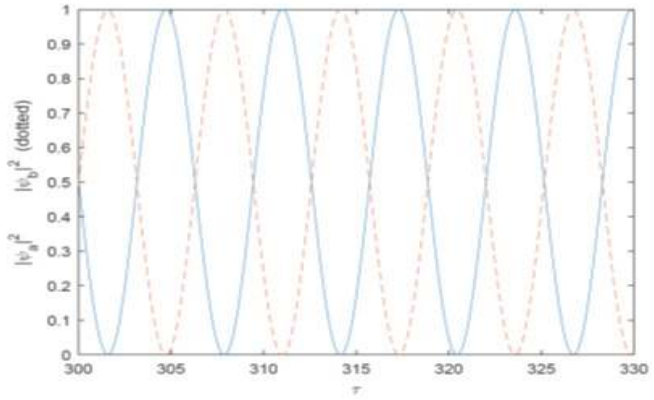

Figure 3: The fast flipping of the two π phase-shifted probabilities $|\psi_{a,b}|^2$ between 0 and 1 when the HDS trajectory crosses the separatrix of Figure 2. This latter is defined by $\delta = \pi/2$ and occurs at 1/4th of the Rabi period, i.e. at $\tau \sim \pi/A = 314$ for $A = 0.01$.

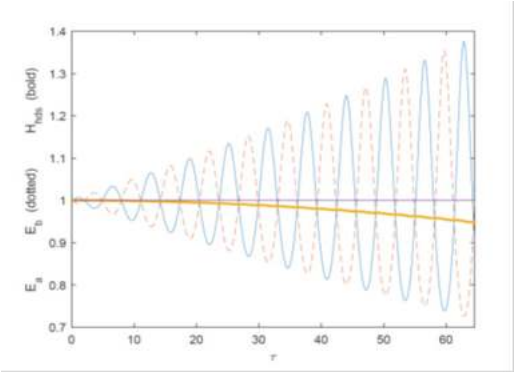

Figure 4: The start of the growing-amplitude oscillations with the short HDS orbit period ~ 2π of the two state energies $E_{a,b}$ which are phase-shifted by π and defined by equations (9) and (11) in the weakly Rabi-driven resonant case $A = 0.01$. The mean qubit energy $\mathcal{H}$ defined by equations (8-12) is displayed in yellow bold.

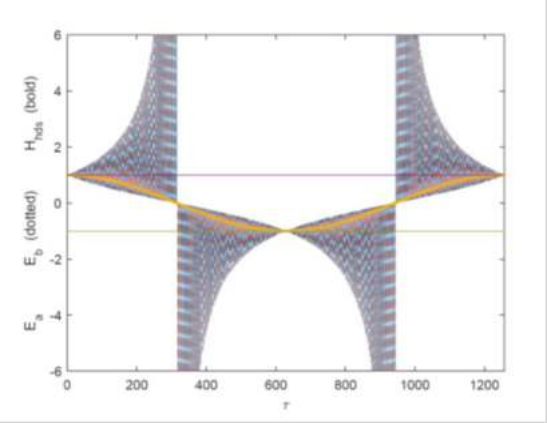

Figure 5: Running on from Figure 4: the high-frequency long-range oscillations of the two state energies E_a (continuous) and E_b (dotted) in the weakly Rabi-driven resonant case $A = 0.01$ with their divergences about the two separatrices. The mean qubit energy $\mathcal{H}$ defined by equations (8-12) is displayed in yellow bold: it is in perfect agreement with Rabi's well-known harmonic oscillation (12) of the resonantly-driven qubit energy between its two eigenvalues ±1.

Note that

$$|\psi_a|^2 E_a - |\psi_b|^2 E_b = KB \propto A \ll 1. \qquad (10)$$

Therefore, the values of the mean state energies are quite close: $|\psi_a|^2 E_a \sim |\psi_b|^2 E_b \sim K\mathcal{H}/2$ while the $E_{a,b}$ state energies themselves are phase-shifted by π: see Figures 3 and 4. In terms of the two phases $\Theta(\tau)$ and $\delta(\tau)$, the state energies $E_{a,b}$ read:

$$\frac{E_a}{K} = -\frac{\hbar}{K}\frac{d\Theta}{dt} = -2\dot{\Theta} \quad ; \quad \frac{E_b}{K} = -\frac{\hbar}{K}\frac{d(\Theta+\delta)}{dt} = -2(\dot{\Theta}+\dot{\delta}). \qquad (11)$$

In the weakly driven case $1 >> A \neq 0$, the state energies $E_{a,b}$ are oscillating very fast with the short HDS orbit period ~ 2π while their amplitudes are strongly increasing: see Figure 4. These latter eventually diverge about the two separatrices: see Figures 5 and 6. These high-frequency divergences are counterbalanced by the appropriate vanishing values of their respective high-frequency state amplitudes $\psi_{a,b}$ as shown by Figures 3 and 6. Therefore they yield (in yellow bold in Figures 4 and 5) Rabi's regular harmonic time dependence of mean energy $\mathcal{H}$:

$$\mathcal{H} \sim \cos\frac{A\tau}{2}, \qquad (12)$$

in accordance with equation (8).
The respective standard deviations $\sigma_{a,b}$ defined by the variance

$$\sigma^2_{a,b}(\tau) = |\psi_{a,b}(\tau)|^2 [E_{a,b}(\tau) - \mathcal{H}(\tau)]^2, \qquad (13)$$

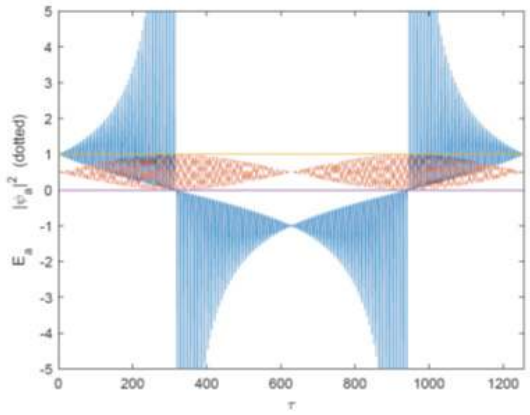

Figure 6: High-frequency growing-amplitude energy E_a defined by equations (9) and (11) together with its high-frequency dotted-brown probability density $|\psi_a|^2$ defined by (2) in the case A = 0.01. The HDS separatrix crossing is zoomed in Figure 3.

describe the range of dispersion of the energy values $\varepsilon(\tau)$ bounded by $\pm\sigma_{a,b}$ about the mean energy $\mathcal{H}$ at the given time τ:

$$\mathcal{H}(\tau) - \sigma_a(\tau) - \sigma_b(\tau) \leq \mathcal{E}(\tau) \leq \mathcal{H}(\tau) + \sigma_a(\tau) + \sigma_b(\tau), \qquad (14)$$

see Figure 7. The darker areas display smaller-amplitude oscillations that are phase-shifted by π with respect to the large-amplitude ones, each oscillation keeping nevertheless its HDS orbit period ~ 2π. The mean energy $\mathcal{H}$ itself is shown in light blue while the (purple $+\sigma_{a,b}$) (resp. green $-\sigma_{a,b}$) high-frequency standard deviations display the rather important dispersion of acceptable energy ε about $\mathcal{H}$ in accordance with (14), except at the two eigenvalues ±1 where, as expected, this dispersion vanishes.

The action-angle HDS description of the quantum Zeno jump

Due to QZE, continuous measurement (by use of photon emission from the 3rd high-rate monitored ancilla level |B>) of the Rabi-stimulated ground state transition to excited state |D> in [15] forces the population —and hence the energy— of ground state ε(τ) ~ −1 to remain quasi-constant in (14) before the transition to the excited state +1 occurs. There is clearly a *QZE vs Rabi* competition between Rabi driving (12) and QZE population freezing [10]. We wish to describe this competition in the energy regions (14) illustrated by the 2nd (r.h.s.) half of the energy phase portrait displayed by Figure 7. Therefore we take the origin of time at τ = $2\pi/A$ = 786 in Figure 7. We recall that the resonant Rabi drive in [15] is very weak like in the present case (actually we assume A = 0.008 in this section). Therefore, the system is quasi-periodic with the *same* ~ 2π time scale of any single HDS quasi-orbit period

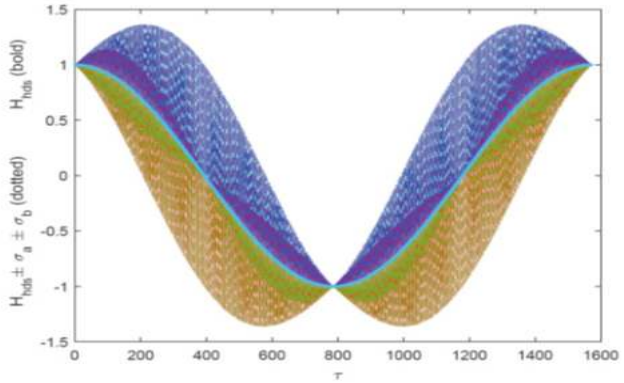

Figure 7: The dressing of the HDS Hamiltonian $\mathcal{H}$ (in continuous light blue) by the standard deviations $\pm\sigma_{a,b}$ defined by equations (13) and (14) in one Rabi period 4π/A defined by A = 0.008.

in our reduced units (7). Hence the corresponding HDS frequency quite close to unity for *all* quasi-orbits illustrated by Figures 1 and 2. This remarkable property suggests to make use of the type-2 canonical transformation from the generalized coordinates δ and α defined by (2) to the new action-angle canonical coordinates whose action defined along the two QZE paths of (quasi)constant energy $\varepsilon(\tau) \sim \mp 1$:

$$S(\tau) = \int_0^\tau \alpha\dot{\delta}\mathrm{d}\tau' = \int_0^\tau \alpha\Big[B - \frac{\alpha\cos\delta}{\sqrt{1-\alpha^2}}\Big]\mathrm{d}\tau'. \quad (15)$$

is respectively conjugated to the trajectory angle ~ ±τ defined by the HDS quasi-orbit frequency ~ ±1. It is displayed by the upper bold profile in Figure 8. The peak occurs about the separatrix crossing at $\tau = \pi/A$ between the $\mathcal{H} < 0$ and the $\mathcal{H} > 0$ cells of the phase space.

Therefore, we respectively define the corresponding action before and after the separatrix as follows [17]:

$$\text{after}: \quad S(\tau) \sim K - \int_{\pi/A}^{\tau<2\pi/A} \big[1 - \mathcal{H}(\tau')\big]\mathrm{d}\tau',$$

$$\text{before}: \quad S(\tau) \sim \int_0^{\tau<\pi/A} \big[1 + \mathcal{H}(\tau')\big]\mathrm{d}\tau' \quad ; \quad (16)$$

where $K = \int_0^{\pi/A} [1 + \mathcal{H}]d\tau$ is the amplitude of the peak.

In order to describe the *QZE* vs Rabi competition in (14), we introduce the following family of possible transitions from the ground state **ε(τ)** ~ −1 to the excited state **ε(τ)** ~ +1 during 1/2 Rabi period $2\pi/A$ = 786. These transitions are parametrized by p:

$$\mathcal{E}_p(\tau) = \frac{1}{\tanh(\pi/Ap)} \tanh\frac{\tau - \pi/A}{p}, \quad (17)$$

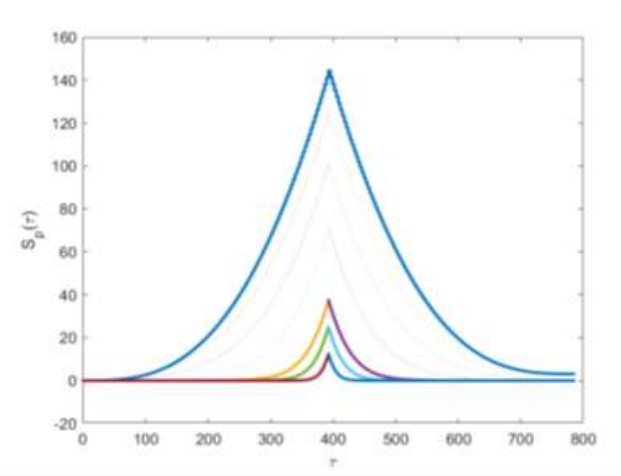

Figure 8: A = 0.008. Upper bold profile: The action defined by equations (15) or (16) when crossing the separatrix at 1/4th of the Rabi period, i.e. here at τ = 394. Three subsequent decreasing dashed profiles: typical action profiles (18) for, say, p=201, 152, 103. The three last lower bold profiles: quantized action (18) corresponding in our reduced units (7) to the maxima K_p = 3h, K_p = 2h and K_p =h where K_p is defined by (19). They respectively correspond to p=53, p=35 and p=17 in equations (17-18). The p=53 action yielding K_{53} = 37.43 and corresponding to the quantized action 3h agrees quite well with the path followed by the jump evolutions shown by Figure 3b of [15]: see Figure 9.

and they occur within the standard deviations (14) that are displayed by the 2nd (r.h.s.) half of Figure 7. We note that p=250 reproduces fairly well mean energy (12). Decreasing p defines sharper and sharper transitions about the separatrix at 1/4 Rabi period $\tau = \pi/A$: see Figure 8. Using (16), we have:

before:

$$S_p(\tau) \sim \int_0^{\tau<\pi/A} \big[1 + \mathcal{E}_p(\tau')\big]\mathrm{d}\tau' \quad ; \quad \text{after}: \quad S_p(\tau) \sim K_p - \int_{\pi/A}^{\tau<2\pi/A} \big[1 - \mathcal{E}_p(\tau')\big]\mathrm{d}\tau', \quad (18)$$

where

$$K_p = \int_0^{\pi/A} [1 + \mathcal{E}_p(\tau)]\mathrm{d}\tau \qquad (19)$$

is the amplitude of the peak of action (18): e.g. $K_{250} = 144$ in Figure 8 since $\varepsilon_{250}(\tau) \sim \mathcal{H}(\tau)$. The smaller p, the lower K_p.

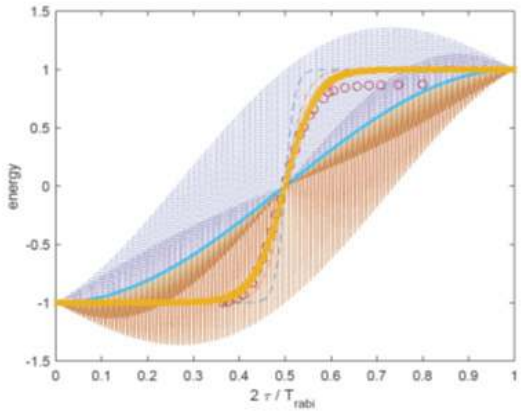

Figure 9: Second (r.h.s.) part of Figure 7. Circles: the path in the Hilbert space followed by the jump evolutions given in Figure 3b of [15] using the $T_{rabi} = 50\ \mu s$ Rabi period given in [15] for the normalization of the τ -axis. The 13% deviation from the excited eigenvalue +1 is due to imperfections, mostly excitations to higher levels [15]. Dashed line, dotted-dashed line and thick yellow bold line: the energy path (17) with $p = 17$, $p = 35$ and $p = 53$ corresponding respectively to the $n = 1$, $n = 2$ and $n = 3$ quantized action (18) in accordance with quantization (20): see Figure 8.

Action quantization

The above action-angle description yieds in the reduced units (7) the following quantization of the generalized momentum (19) at the separatrix crossing:

$$K_p = n\,h = 2\pi n\hbar = 4\pi n \quad \text{where} \quad n = 1,\ 2,\ 3\,...(20)$$

Decreasing p from 250 —where $\boldsymbol{\varepsilon}_{250} \sim \mathcal{H}$ reproduces the Rabi oscillation (12)— to the particular values $p_{1,\,2,\,3...}$ such that the corresponding maxima $Kp_{1,\,2,\,3...} = 4\pi$, 8π, 12π... in accordance with (20) leads to the three lower bold profiles of Figure 8. We respectively find $p_1 = 17$, $p_2 = 35$ and $p_3 = 53$ for $n = 1$, $n = 2$ and $n = 3$. The corresponding energy trajectories $\boldsymbol{\varepsilon}_{p1,\,2,\,3...}(\tau)$ defined by (17) are shown in Figure 9: dashed line for n = 1, dotted dashed line for $n = 2$ and bold yellow line for $n = 3$. The observed "times-of-flight" between the two eigenvalues ±1 in Figure 3b of [15] are reproduced by circles in Figure 9, using the $T_{rabi} = 50$ μs value of the Rabi period given in this paper. Its 13% deviation from the excited eigenvalue +1 is due, the authors say, to imperfections, mostly excitations to higher levels. We conclude that there is a quite good agreement between Ref. [15]'s "time-of flight" circled data in Figure 9 and the $n = 3$ discrete action trajectory defined by $p = 53$ in (17). The fact that [15] stimulates this specific third quantized action is probably due to particular choices in the experimental conditions. A challenging experimental confirmation of the present theory would be to obtain by use of a similar *Rabi vs QZE* qubit stimulation set-up the sharper $n = 1$ and/or $n = 2$ transitions.

Conclusion

We explain the *QZE vs Rabi* transitions (or "Quantum Zeno Jumps") between the two Rabi-driven states of a continuously-observed qubit by both QZE and action quantization within the standard deviation of the system energy about its Rabi harmonic mean value. The equivalence between the quantum description of a driven qubit and its dual non-autonomous HDS Hamiltonian model [17] allows the type-2 canonical transformation from the generalized HDS coordinates δ and α to new action-angle coordinates. These latter yield the sharp action variation when the HDS trajectory crosses the separatrix of the system. This value is quantized and yields nh. We find that the n = 3 quantized solution agrees quite well with the QZE "time-of-flight" data given in [15]. This reference displays the observation and explanation of several other spectacular effects that we did not consider in the present simple theory; e.g. the mid-flight transition reversal as well as the fine-structure of the Rabi driving process in the dynamics of the transition. Our aim is merely to show that it suffices to explicitely refer to QZE and in addition to make use of action quantization for explaining the anomalous quantum Zeno jump described in the remarkable experiment [15]. This constitutes a new result in the debate concerning the interpretation of this experiment [12]. The agreement between Ref. [15]'s quite accurate description in terms of the theory of quantum trajectories and our empirical action-angle description in terms of *Rabi-vs-QZE* competition emphasizes the profound coherence of the quantum theory.

Acknowledgments

The author gratefully acknowledges financial and technical support from UMR *Lagrange* (Observatoire de la Côte d'Azur, université de Nice, France) as well as from the Icelandic Technology Development Fund (University of Iceland, Reykjavik, Iceland). He feels indebted to M. Devoret for his validation of the existence of QZE in experiment [15].

References

1. B. B. Misra and E. Sudarshan. (1977). The Zero's paradox in quantum theory. *J. Math. Phys.* 18, 756.
2. Home, D., & Whitaker, M. A. B. (1993). A unified framework for quantum Zeno processes. *Physics Letters A,* 173(4-5), 327-331.
3. Itano, W. M. (2019). The quantum Zeno paradox, 42 years on. Current Science, 116(2), 201.
4. Pascazio, S., Namiki, M., Badurek, G., & Rauch, H. (1993). Quantum Zeno effect with neutron spin. *Physics Letters A,* 179(3), 155-160.
5. Ballentine, L. E. (1991). Comment on ''quantum Zeno effect''. *Physical Review A*, 43(9), 5165.
6. Petrosky, T., Tasaki, S., & Prigogine, I. (1991). Quantum zeno effect. Physica A: *Statistical Mechanics and its Applications,* 170(2), 306-325.
7. Petrosky, T., Tasaki, S., & Prigogine, I. (1991). Quantum zeno effect. Physica A: *Statistical Mechanics and its Applications,* 170(2), 306-325.
8. von Neumann, J. (1932). Mathematische Grundlagen der Quantenmechanik Springer.
9. Cook, R. J. (1988). What are quantum jumps?. *Physica Scripta*, 1988(T21), 49.
10. Itano, W. M., Heinzen, D. J., Bollinger, J. J., & Wineland, D. J. (1990). Quantum zeno effect. *Physical Review A*, 41(5), 2295.

11. Porrati, M., & Putterman, S. (1987). Wave-function collapse due to null measurements: The origin of intermittent atomic fluorescence. *Physical Review A*, 36(2), 929.
12. J. M. Raimond, La Recherche 555, 41 (2020).
13. Dalibard, J., Castin, Y., & Mølmer, K. (1992). Wave-function approach to dissipative processes in quantum optics. *Physical review letters,* 68(5), 580.
14. Dum, R., Zoller, P., & Ritsch, H. (1992). Monte Carlo simulation of the atomic master equation for spontaneous emission. *Physical Review A*, 45(7), 4879.
15. Minev, Z. K., Mundhada, S. O., Shankar, S., Reinhold, P., Gutiérrez-Jáuregui, R., Schoelkopf, R. J., ... & Devoret, M. H. (2019). To catch and reverse a quantum jump mid-flight. *Nature,* 570(7760), 200-204.
16. M. Devoret, private communication, feb 13, 2020.
17. Reinisch, G. (1998). Classical Hamiltonian description of a two-level quantum system: The quantum Zeno effect. *Physica D: Nonlinear Phenomena,* 119(3-4), 239-249.
18. Rauch, H., Zeilinger, A., Badurek, G., Wilfing, A., Bauspiess, W., & Bonse, U. (1975). Verification of coherent spinor rotation of fermions. *Physics Letters A*, 54(6), 425-427.
19. Werner, S. A., Colella, R., Overhauser, A. W., & Eagen, C. F. (1975). Observation of the phase shift of a neutron due to precession in a magnetic field. *Physical Review Letters*, 35(16), 1053.
20. Klein, A. G., & Opat, G. (1976). Observation of 2 π rotations by Fresnel diffraction of neutrons. *Physical Review Letters,* 37(5), 238.
21. Deutsch, I. H. (2020). Harnessing the power of the second quantum revolution. *PRX Quantum*, 1(2), 020101.
22. Reinisch, G. (1998). Random phase dynamics in resonantly driven spin one-half systems. *Physics Letters A,* 238(2-3), 107-111.